Orthogonal Wavelet Analysis of Flow Structures in Asymmetric Wakes

S. Fujimoto and A. Rinoshika

Abstract The turbulent wake structures of various scales generated by an asymmetric bluff body have been experimentally investigated in this paper. Firstly, the instantaneous velocity and vorticity of turbulent wake were measured by the high-speed PIV technique at a Reynolds number of 8,960 in the circulating water channel. In order to decompose turbulent structures into a number of subsets based on their central frequencies, one- and two-dimensional wavelet multi-resolution technique is then used to analyze the instantaneous velocity and vorticity. It is found that the large-scale turbulent structure makes the largest contribution to the vorticity and Reynolds shear stresses. However, the small-scale structures make less contribution to the vorticity and Reynolds shear stresses.

Keywords PIV · Orthogonal wavelet multi-resolution technique · Reynolds shear stress · Vorticity · Wake

1 Introduction

It is a well-known fact that the turbulent wakes generated by a bluff body cause the aerodynamic drag, vibration, and noise. Until now, the most investigations focus on the symmetry bluff body wake, and the topology and transport characteristics of the turbulent structure in the wake flow have been well established (Hussain and Hayakawa 1987; Lin et al. 1996; Wei and Smith 1986). Recently, the multi-scale structures of various wakes are revealed based on the orthogonal wavelet multi-resolution analysis of the hot-wire data and PIV data (Rinoshika and Omori 2011;

S. Fujimoto · A. Rinoshika (✉)
Department of Mechanical Systems Engineering, Yamagata University, Yamagata, Japan
e-mail: rinosika@yz.yamagata-u.ac.jp

Y. Zhou et al. (eds.), *Fluid-Structure-Sound Interactions and Control*,
Lecture Notes in Mechanical Engineering, DOI: 10.1007/978-3-642-40371-2_8,

Rinoshika and Zhou 2005a, 2005b, 2009). However, there is little research on the multi-scale turbulent wakes generated by an asymmetric bluff body which will provide important information in industrial applications, thus becoming an objective of the present work.

In this study, the high-speed PIV was applied to measure a turbulent wake generated by an asymmetric body. Then, one- and two-dimensional wavelet multi-resolution technique was used to analyze the instantaneous velocity and vorticity. The turbulent structures were decomposed into a number of subsets based on their central frequencies. The contributions from the turbulent structures of various scales to Reynolds shear stresses and vorticity were examined.

2 Experimental Details

In this study, a compound of 1/4 circular and triangle cylinders is designed for the purpose of both reducing aerodynamic drag and producing a downward force. As a fundamental research, a two-dimensional asymmetric model having a scale of $L = 50$ mm and aspect ratio of eight with respect to their whole length, as shown in Fig. 1, is used as a wake generator. The experiment was conducted in a circulating water channel, which has 400 (width) × 200 (height) × 1,000 mm (length) working section. The high-speed PIV measurement system, as shown in Fig. 2, was carried out at a constant free stream velocity of $U_0 = 0.19$ m/s, corresponding to Reynolds number Re ($\equiv U_0 L/\nu$) = 8,960.

Polystyrene particles with a diameter of 63–75 μm were seeded in the flow loop as PIV tracers. A high-speed camera (Photoron FASTCAM SA3) and a laser light sheet were used to capture the digital images at a frame rate of 500 fps (frame per second) with a resolution of 1,024 × 1,024 pixels and the shutter speed of each frame was set at 1 ms. 1,025 digital images were analyzed by ProVision PIV software. The measured flow area is about 200 × 200 mm behind bluff body.

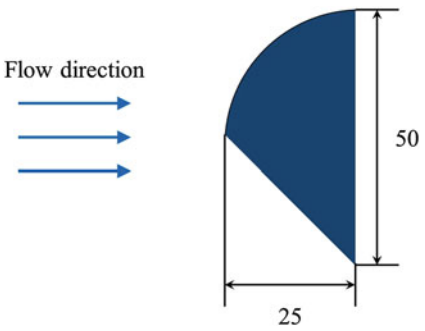

Fig. 1 Experimental model

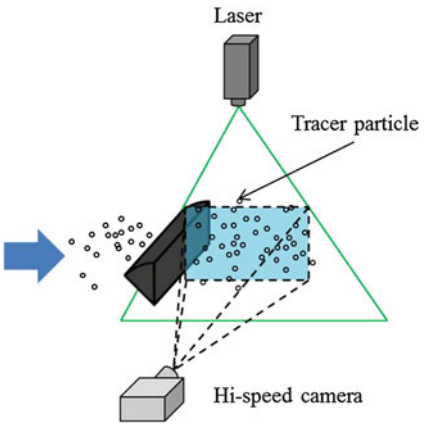

Fig. 2 Experimental setup

3 Orthogonal Wavelet Multi-resolution Technique

In this study, the discrete serial data are decomposed into a number of wavelet components based on characteristic frequencies by using an orthogonal wavelet multi-resolution technique. As an example, a one-dimensional wavelet multi-resolution technique is briefly described in this section. A one-dimensional orthogonal discrete wavelet transform is often defined in matrix form by

$$\boldsymbol{S} = \boldsymbol{W}\boldsymbol{X} \tag{1.1}$$

where $\boldsymbol{X}$ is a one-dimensional data matrix. $\boldsymbol{S}$ and $\boldsymbol{W}$ are called the orthogonal wavelet coefficient matrix and the analyzing wavelet matrix, respectively. $\boldsymbol{W}$ is orthogonal. Therefore, the orthogonal discrete wavelet transform has the inverse transform, which is given by

$$\boldsymbol{X} = \boldsymbol{W}^T\boldsymbol{S} \tag{1.2}$$

In order to decompose the serial data into the grouped frequency components, the inverse wavelet transform is applied to the discrete wavelet coefficients at each level. This decomposition method is called the wavelet multi-resolution analysis and can be written as

$$\boldsymbol{X} = \boldsymbol{W}^T\boldsymbol{S}_1 + \boldsymbol{W}^T\boldsymbol{S}_2 + \ldots + \boldsymbol{W}^T\boldsymbol{S}_N \tag{1.3}$$

In this study, the Daubechies wavelet matrix with an order of 12 is used as the analyzing wavelet matrix. In case of two-dimensional wavelet multi-resolution analysis, wavelet coefficient matrix $\boldsymbol{S}$ is additionally transformed by $\boldsymbol{W}$ from another direction and wavelet multi-resolution analysis can be written as

$$\boldsymbol{X} = \boldsymbol{W}^T\boldsymbol{S}_1\boldsymbol{W} + \boldsymbol{W}^T\boldsymbol{S}_2\boldsymbol{W} + \ldots + \boldsymbol{W}^T\boldsymbol{S}_N\boldsymbol{W} \tag{1.4}$$

where the first term $\boldsymbol{W}^T\boldsymbol{S}_1\boldsymbol{W}$ and the last term $\boldsymbol{W}^T\boldsymbol{S}_N\boldsymbol{W}$ represent the data components at wavelet level 1 and level N, respectively. It is evident that the sum of all wavelet components can be used to reconstruct the original data in the case of the orthogonal wavelet bases.

4 Results and Discussion

4.1 Reynolds Shear Stress and Instantaneous Flow Structures

Figure 3 shows the distribution of the normalized Reynolds shear stress contours of $\overline{uv}/U_0^2$ calculated by the measured instantaneous velocity, and instantaneous streamlines and normalized vorticity contour, $\omega_z L/U_0$. The color mappings have been assigned to the Reynolds shear stress and the vorticity values and the highest concentration is displayed as red and the lowest as blue, respectively. The distributions of $\overline{uv}/U_0^2$ exhibit the maximum values near the end of the separation region. The positive Reynolds shear stress of downside is more widely distributed than the negative Reynolds shear stress on the upside, suggesting the effect of the asymmetric body, and the lower side of body generates the high-intensity turbulence.

The asymmetric large-scale vortices with opposite sense of rotation shed from body are clearly observed. The large-scale spanwise structures originated from the lower (triangle) side become weak due to the effect of "rolls" structures shed from the upper (circle) side. It would be difficult to study the behaviors of the structures other than the large-scale ones.

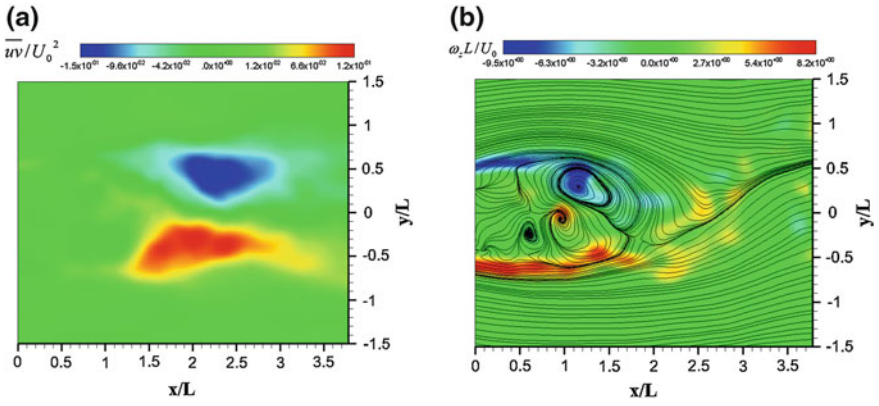

Fig. 3 Asymmetric wake structure measured by PIV analysis

4.2 Reynolds Shear Stress of Different Wavelet Components

Figure 4 presents the normalized Reynolds shear stress contours of $\overline{uv}/U_0^2$ calculated from the wavelet components of the instantaneous fluctuation velocity at wavelet levels 1 and 7. The distributions of $\overline{uv}/U_0^2$ at level 1 exhibit the maximum values near the end of the separation region, corresponding well to the measured Reynolds shear stress contour. It indicates that the most significant contribution to the Reynolds shear stress comes from the large-scale structures, accounting for almost 76–83 % of the measured maximum $\overline{uv}/U_0^2$. At the level 7, the maximum Reynolds shear stress further decreases and only appears near the asymmetric body. It implies that less contribution to the Reynolds shear stresses comes from the small-scale structures.

4.3 Instantaneous Flow Structures of Different Wavelet Components

Figure 5 shows the two-dimensional streamlines and vorticity contours of the wavelet components at level 1, level 2, and levels 3 and 4. The streamlines and vorticity contours at level 1 coincide approximately with the measured data of Fig. 3b, implying the large-scale structures make the most contribution to the flow structure, and distinguishing vortex except redundant data is observed clearly. It is obvious that the large-scale structure is the energy-containing structure. At level 1, the body downside generates high positive vorticity and distributes widely. At level 2, as shown in Fig. 5b, relatively intermediate-scale structures are observed near the body. Compared with the vorticity of large-scale components, the strength

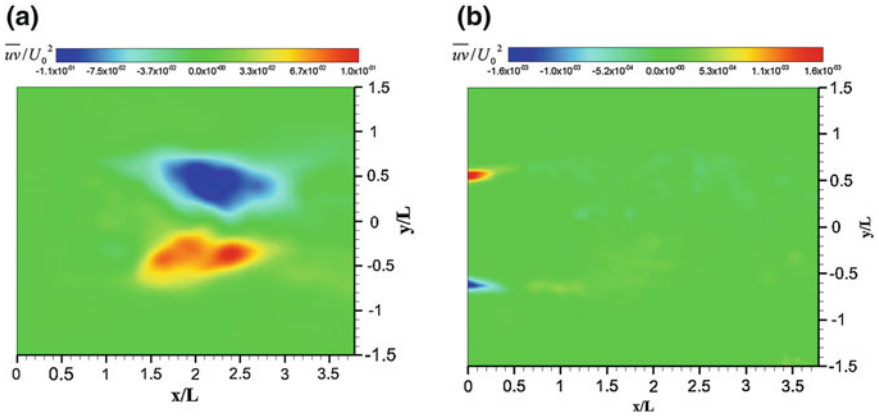

Fig. 4 Reynolds shear stress contours of various wavelet components

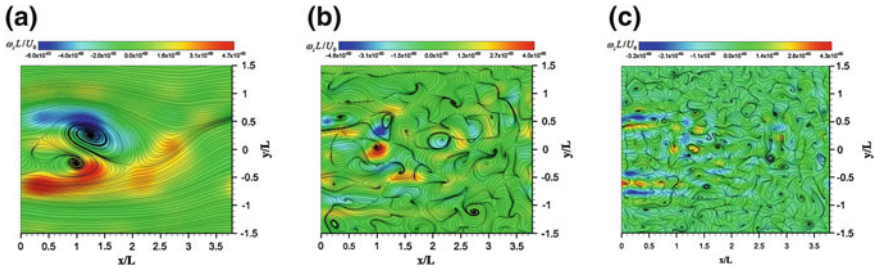

Fig. 5 Streamlines and vorticity contours of various wavelet components

of the intermediate-scale component decreases. For the small-scale vorticity at levels 3 and 4, the small-scale structures are observed in the entire flow field. Especially, many strong vorticity peaks appear in the shear layer of separation region.

5 Conclusion

In this study, the following results can be drawn:

1. The maximum Reynolds shear stresses are distributed near the end of the separation region, and the lower side of asymmetric body generates the high-intensity turbulence.
2. The large-scale turbulent structures make the largest contribution to the Reynolds shear stress and vorticity. The contributions to the Reynolds shear stress from large-scale turbulent structures have a proportion of 76–83 % to the measured maximum Reynolds shear stress.
3. The small-scale structures are observed in all flow fields and the maximum Reynolds shear stress and vorticity appear in the separation shear layer. However, the small-scale structures make less contribution to Reynolds shear stresses and vorticity.

References

Hussain AKMF, Hayakawa M (1987) Education of large-scale organized structures in a turbulent plane wake. J Fluid Mech 108:193–229

Lin J-C, Vorobieff P, Rockwell D (1996) Space-time imaging of a turbulent near-wake by high-image-density particle image cinematography. Phys Fluids 8:555–564

Rinoshika A, Omori H (2011) Orthogonal wavelet analysis of turbulent wakes behind various bluff bodies. Exp Thermal Fluid Sci 35:1231–1238

Rinoshika A, Zhou Y (2005a) Orthogonal wavelet multi-resolution analysis of a turbulent cylinder wake. J Fluid Mech 524:229–248

Rinoshika A, Zhou Y (2005b) Effects of initial conditions on a wavelet-decomposed turbulent near-wake. Phys Rev E 71(046303):1–8

Rinoshika A, Zhou Y (2009) Reynolds number effects on wavelet components of self-preserving turbulent structures. Phys Rev E 79(046332):1–11

Wei T, Smith CR (1986) Secondary vortices in the wake of circular cylinders. J Fluid Mech 169:513–533